

Geometric properties of acoustic waves generated by a point source in solar-like interior: effects of acoustic cut-off frequency.

S. Zharkov^{1,2*}

¹*Department of Physics and Mathematics, University of Hull, Cottingham Road, Kingston-upon-Hull, HU6 7RX, UK*

²*Mullard Space Science Laboratory, University College London, Holmbury St. Mary, Dorking, RH5 6NT, UK*

ABSTRACT

Acoustic waves generated by a point source in stratified plasma are considered in this paper. Analytical parametric solution for monochromatic source is derived for plane-parallel polytrope model of the solar interior. The solution is used to gain insight into the properties of the generated wavefront as a function of excitation frequency and depth. A slowly varying pressure perturbation moving in upper layers of solar photosphere with supersonic speed is also considered. It is shown to excite acoustic waves putting certain restrictions upon their geometry of the generated wavefront. The results are discussed in relation to flare generated sunquakes.

Key words: methods: analytical — Sun: photosphere — Sun: helioseismology — Sun: oscillations

1 INTRODUCTION

Ray theory, as form of geometrical optics, has played a crucial role in helioseismology of acoustic oscillations, laying foundations to such methods as time-distance helioseismology (Duvall et al. 1993; Kosovichev & Duvall 1997; Giles 2000; D’Silva & Duvall 1995; D’Silva 1996; Thompson & Zharkov 2008), acoustic holography (Lindsey & Braun 2000; Lindsey & Braun 2004) and far-side imaging (Lindsey & Braun 2000). It has provided us with rich insight into the nature of acoustic wave propagation in the Sun from properties of low-degree modes and Duvall’s law used in global helioseismology to averaging setups and focusing information relied upon in local helioseismic techniques. While more accurate numerical methods have since been deployed for computing helioseismic sensitivity kernels, which are used to deduce subsurface properties of the solar interior from observations, these have generally confirmed and built on earlier results from ray-theory (Couvidat et al. 2004, 2006).

Nonetheless, the use of ray-theory in solar physics has mostly centred on studies of individual rays, or modes, with little attention paid to fully transcribing the initial conditions responsible for generating the family of rays that fully describes the wavefield. For example, Bogdan (1997) has compared the relationship between the modal and time-distance formulations of local helioseismology, but by own admission neglecting to take into account the initial value problem in terms of ray theory. One of the simplest of such cases is a spherical monochromatic point source, which is considered in this paper.

When applied to standard wave-equation the mathematical method of geometric optics is known by other names such as De-

bye ray-theory, geometric acoustics, geometric seismics, WKB or semiclassical approximation leading to a fair amount of confusion. In solar physics some of the more rigorous applications of the method can be found in works by Gough (1993, 2007, and references therein).

Here I use purely mathematical approach as set out by Kravtsov & Orlov (1990) for standard wave-equation and generalised for general asymptotic differential operators by Guillemin & Sternberg (1990) to explicitly derive and interpret the eikonal and transport equations for non-linear wave equation in the presence of acoustic cut-off frequency. Finding the full solution of the problem depends on reconstruction of the phase function throughout the whole domain which is accomplished by solving the eikonal equation. The phase function defines the geometry of the problem and can be found when proper initial conditions are prescribed. I then find such solution for the point source using basic polytrope model of the solar interior and consider its basic properties such as wavefront geometry, caustics and surface manifestations.¹

For physical applications, the results are compared with known acoustic sources in the Sun. Stochastic turbulent convection in the upper layers of the convective zone is generally thought to generate most of the solar acoustic spectrum. However, another known source of sound waves in the Sun are acoustically active solar flares. In such flares, the energy release in the corona generates observable photospheric ripples that accelerate radially outward from a source region. This recently discovered phenomena known

¹ Note that there are also other independent means of deriving the eikonal equation such as Fourier transform and stationary phase method (Chapman et al. 1999; Felsen & Marcuvitz 1991).

* E-mail: s.zharkov@hull.ac.uk

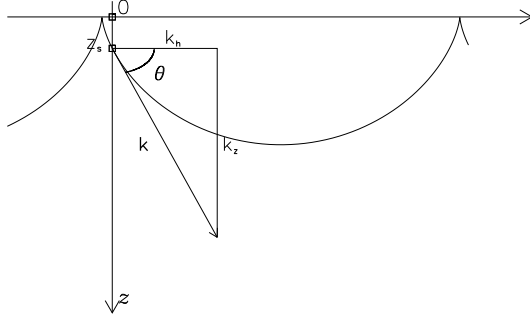


Figure 1. Spatial geometry of the problem

as 'sunquake' (Kosovichev & Zharkova 1998) provides us with a localised example of wave excitation in the Sun. The acoustic nature of sunquake photospheric ripples has been well established and localisation of the source position can be deduced with good precision using helioseismic techniques such as time-distance analysis (Kosovichev & Zharkova 1998; Kosovichev 2006, 2007) and acoustic holography Donea et al. (1999); Donea & Lindsey (2005); Lindsey & Donea (2008). In particular, the egression computation in acoustic holography uses the Green's function built on the assumption of a monochromatic point source generating downward propagating waves from given depth in the solar atmosphere.

The paper is organised as follows the mathematical formalism for asymptotical treatment and solution of the solar wave equation, splitting it into eikonal and transport equations is described in Section 2. The link between general solution and initial conditions is addressed in 3. The solution for eikonal equation for a point source is derived in Section 4 including the expression for the Jacobian. Possible applications and limitations of the derived solutions to sun-quakes and basic properties of moving source wave-fronts are discussed in Section 5.

2 EQUATION FOR SCALED PRESSURE PERTURBATION AND GEOMETRICAL ASYMPTOTICS

Solar wave equation for scaled Lagrangian pressure perturbation, $\Psi = \rho_0^{-\frac{1}{2}} \delta p$, can be written (Gough 1993) as

$$\frac{1}{c^2} \frac{\partial^2}{\partial t^2} \left(\frac{\partial^2}{\partial t^2} + \omega_{ac}^2 \right) \Psi - \frac{\partial^2}{\partial t^2} \nabla^2 \Psi - N^2 \nabla_h^2 \Psi = 0. \quad (2.1)$$

Here ∇_h^2 is the horizontal Laplacian operator, ρ_0 unperturbed quiet sun density, c^2 adiabatic sound speed, N^2 Brunt-Vaasala buoyancy frequency, and

$$\omega_{ac}^2 = \frac{c^2}{4H_\rho^2} (1 - 2\mathbf{n} \cdot \nabla H_\rho) \quad (2.2)$$

is Lamb's acoustic cut-off frequency, defined in terms of density scale height H_ρ and unit vector \mathbf{n} in the direction of the gravity action. As is standard in acoustic mode helioseismology let us take $N^2 = 0$ to simplify the equation to a non-linear second-order wave-equation:

$$\frac{1}{c^2} \left(\frac{\partial^2}{\partial t^2} + \omega_{ac}^2 \right) \Psi - \nabla^2 \Psi = 0 \quad (2.3)$$

To find asymptotic solutions the method of geometrical optics

(Kravtsov & Orlov 1990) is used in this paper. The method, developed for linear wave-equation and generalised as method of Geometric Asymptotics by Guillemin & Sternberg (1990) for a wider range of high order differential operators. In short, this works by looking for the solution of the equation (2.3) in terms of Debye ray series (or WKB ansatz Chapman et al. (1999)) written for asymptotically large parameter Λ :

$$\Psi(\mathbf{r}, t) = \sum_m \frac{A_m(\mathbf{r}, t)}{(i\Lambda)^m} e^{i\Lambda\varphi(\mathbf{r}, t)}. \quad (2.4)$$

On substitution of the series into (2.3) and arranging the result in terms powers of the large asymptotic parameter Λ a series of equations is obtained:

$$|\nabla\varphi|^2 - \frac{1}{c^2} \left| \frac{\partial\varphi}{\partial t} \right|^2 + \frac{\omega_{ac}^2}{c^2} = 0 \quad (2.5a)$$

$$2 \nabla A_0 \cdot \nabla \varphi + A_0 \nabla^2 \varphi - \frac{2}{c^2} \frac{\partial\varphi}{\partial t} \frac{\partial A_0}{\partial t} - \frac{1}{c^2} A_0 \frac{\partial^2 \varphi}{\partial t^2} = 0 \quad (2.5b)$$

$$2 \nabla A_1 \cdot \nabla \varphi + A_1 \nabla^2 \varphi - \frac{2}{c^2} \frac{\partial\varphi}{\partial t} \frac{\partial A_1}{\partial t} - \frac{1}{c^2} A_1 \frac{\partial^2 \varphi}{\partial t^2} = - \left(\nabla^2 - \frac{1}{c^2} \frac{\partial^2}{\partial t^2} \right) A_0 \quad (2.5c)$$

...

Here (2.5a) is a first order differential equation in partial derivatives called an eikonal equation which under suitable initial conditions can be solved to fully reconstruct phase function $\varphi(\mathbf{r}, t)$, which is also known as eikonal. The following (2.5b-2.5c) are called transport equations and can be solved iteratively using the solution for eikonal to obtain amplitude coefficients A_0, A_1, \dots . For more details and examples of the application of the method in the solar case see Gough (1993).

Let M be a space-time manifold, described by Cartesian coordinates (x, y, z) and time, t . Let z be the depth, and x and y correspond to horizontal directions. Then, as $\varphi = \varphi(x, y, z, t)$, the following variables describe φ in the phase space, ΩM

$$k_x = \frac{\partial\varphi}{\partial x}, \quad k_y = \frac{\partial\varphi}{\partial y}, \quad k_z = \frac{\partial\varphi}{\partial z}, \quad \omega = -\frac{\partial\varphi}{\partial t}. \quad (2.6)$$

The eikonal (2.5a) belongs to the class of Hamilton-Jacobi equations and can be solved by method of characteristics in the phase space. In the above notation it corresponds to the Hamiltonian

$$H = \frac{1}{2} \left(k_x^2 + k_y^2 + k_z^2 - \frac{\omega^2 - \omega_{ac}^2}{c^2} \right), \quad (2.7)$$

so that the equation (2.5a) becomes $H = 0$ and finding the solution is reduced to integration of the characteristic system.

It can be shown (see Section 3.2 for example) that when the Hamiltonian (2.7) does not explicitly depend on horizontal variables, under suitably symmetric initial conditions, M can be reduced by one dimension, so that the solution can primarily be sought in two spatial dimensions, i.e. $\varphi = \varphi(x, z, t)$, so that

$$H = \frac{1}{2} \left(k_h^2 + k_z^2 - \frac{\omega^2 - \omega_{ac}^2}{c^2} \right), \quad (2.8a)$$

$$k_h = \frac{\partial\varphi}{\partial x}, \quad k_z = \frac{\partial\varphi}{\partial z}, \quad \omega = -\frac{\partial\varphi}{\partial t}. \quad (2.8b)$$

The full solution is then obtained via rotation using $k_h^2 = k_x^2 + k_y^2$ relationship.

In the problems considered in this paper, the sound speed and acoustic cut-off frequency depend only on depth, so the time-dependent equation (2.3) is often reduced to two spatial dimensions

plus time. In such case we introduce cartesian coordinates x and z on manifold M , corresponding to horizontal and vertical directions, with depth z chosen to be 0 at the surface and positive below it (see Figure 1). Note that in six dimensional space ΩM the graph of φ (i.e. the map $(x, z, t) \mapsto (x, z, t, \frac{\partial \varphi}{\partial x}, \frac{\partial \varphi}{\partial z}, \frac{\partial \varphi}{\partial t})$) is a three-dimensional surface. The characteristic system is then defined as

$$\begin{cases} \frac{dx}{d\tau} = \frac{\partial H}{\partial k_h}, & \frac{dz}{d\tau} = \frac{\partial H}{\partial k_z}, & \frac{dt}{d\tau} = -\frac{\partial H}{\partial \omega}, \end{cases} \quad (2.9a)$$

$$\begin{cases} \frac{dk_h}{d\tau} = -\frac{\partial H}{\partial x}, & \frac{dk_z}{d\tau} = -\frac{\partial H}{\partial z}, & \frac{d\omega}{d\tau} = \frac{\partial H}{\partial t}, \end{cases} \quad (2.9b)$$

where τ is an independent variable. Note that condition $H = 0$ can be used instead of one of the equations in the above system. Solutions of the system (2.9) written in terms of τ (i.e. $x(\tau), z(\tau), t(\tau), k_h(\tau), k_z(\tau), \omega(\tau)$) provide us with characteristic lines lying on the graph of φ in ΩM . The phase function is determined by integrating

$$\frac{d\varphi}{d\tau} = k_h \frac{dx}{d\tau} + k_z \frac{dz}{d\tau} - \omega \frac{dt}{d\tau} \quad (2.10)$$

along each such line. In order to reconstruct the phase function φ in the whole (x, z, t) domain, initial conditions on some two-dimensional surface $S \in \Omega M$ have to be provided so that characteristic lines originating from every point of such surface sweep out the three-dimensional graph. Let (ζ, η) be the coordinates on S so that the initial field can be written as

$$\Psi_0(\zeta, \eta) = e^{i\Lambda\varphi(\zeta, \eta)} \sum \frac{A_m^0(\zeta, \eta)}{(i\Lambda)^m}.$$

Characteristic solutions of (2.9) with initial conditions taken as described sweep out a three-dimensional surface in ΩM described by (ζ, η, τ) which are called ray-coordinates. Thus, it is important to take into account the proper initial conditions in order to understand the geometrical aspects of the wave-field associated with the equation (2.5a). Projections of individual characteristics $(x(\tau), z(\tau), t(\tau), k_h(\tau), k_z(\tau), \omega(\tau))$ from ΩM onto (x, z, t) space are called rays.

Once the eikonal equation solved, its solution can then be used to reconstruct amplitude along the rays by rewriting the transport equations in ray coordinates. These take form:

$$\frac{dA_0^2}{d\tau} + A_0^2 \frac{d \ln \mathcal{D}(\tau)}{d\tau} = 0, \quad (2.11a)$$

$$2 \frac{dA_1}{d\tau} + A_1 \frac{d \ln \mathcal{D}(\tau)}{d\tau} = - \left(\nabla^2 A_0 - \frac{1}{c^2} \frac{\partial^2 A_0}{\partial t^2} \right), \quad (2.11b)$$

...

Here $\mathcal{D}(\tau) = \frac{\partial(x, z, t)}{\partial(\zeta, \eta, \tau)}$ is the Jacobian of the transform from cartesian to ray coordinates. Zero-order equation has the solution (Kravtsov & Orlov 1990):

$$A_0(\zeta, \eta, \tau) = A_0^0(\zeta, \eta) \left[\frac{\mathcal{D}(\tau_0)}{\mathcal{D}(\tau)} \right]^{\frac{1}{2}}. \quad (2.12)$$

Note that A_0 depends only on geometry of the problem and the initial values of the field along the ray, thus expressing the local character of zero-order WKB approximation. So for example, in order to reconstruct the field at some point (x_1, z_1, t_1) , one normally determines rays coordinates corresponding to that point via eikonal equation solution and then uses (2.12) to find the value of A_0 and (2.10) to find the phase-function.

Higher order coefficients can be written as

$$A_m = A_m^0 \left[\frac{\mathcal{D}(\tau_0)}{\mathcal{D}(\tau)} \right]^{\frac{1}{2}} - \frac{1}{2\sqrt{\mathcal{D}(\tau)}} \times \int_{\tau_0}^{\tau} \left(\nabla^2 A_{m-1} - \frac{1}{c^2} \frac{\partial^2 A_{m-1}}{\partial t^2} \right) \sqrt{\mathcal{D}(\tau)} d\tau'. \quad (2.13)$$

The presence of the Laplacian and higher order time derivative in the integral on the right hand side in the above means that A_m depends not only on the values of A_{m-1} immediately on the ray, but also the values A_{m-1} in ray vicinity. Thus higher order amplitudes describe diffraction effects discarded in zero-order approximation.

At points where the Jacobian is zero, A_0 and higher order coefficients grow infinitely large, thus defining regions where the method breaks down. Such regions require separate analysis such as matching asymptotics or other methods (Kravtsov & Orlov 1990; Kravtsov & Orlov 1993). Points where the Jacobian is zero are said to form caustic surfaces, or caustics. Such surfaces envelope ray surfaces and are singularities of projection of the graph of $\varphi(\zeta, \eta, \tau)$ from ΩM to (x, z, t) space (Arnold 1978).

It is common in many applications to disregard the non-zero order terms in (2.4), $A_m = 0, \forall m > 0$, thus assuming the wave-equation (2.3) solution to be an "eikonal approximation" $\Psi \approx A_0 \exp(i\Lambda\varphi)$, also known as an "almost plane wave". Kravtsov & Orlov (1990); Gough (2007) give necessary conditions for this as that the medium, c^2 and ω_{ac}^2 varies slowly over the characteristic length-scale of variation of the wave.

3 INITIAL CONDITIONS

3.1 General approach

In 3 + 1 dimensions consider initial surface $S \subset M$ parametrised by some coordinate set (θ, ϕ, t_0) , with M described by (x, y, z, t) . Then the field on such surface can be written as

$$\Psi_0(\theta, \phi, t_0) = A_0(\theta, \phi, t_0) e^{i\varphi_0(\theta, \phi, t_0)}. \quad (3.1)$$

Solution of the 3D characteristic system

$$\begin{cases} \frac{d\mathbf{x}}{d\tau} = \frac{\partial H}{\partial \mathbf{k}}, \\ \frac{d\mathbf{k}}{d\tau} = -\frac{\partial H}{\partial \mathbf{x}}, \end{cases} \quad (3.2a)$$

$$\frac{d\mathbf{k}}{d\tau} = -\frac{\partial H}{\partial \mathbf{x}}, \quad (3.2b)$$

deduced from the Hamiltonian (2.7), provides the graph of φ ,

$$\left(x, y, z, t, \frac{\partial \varphi}{\partial x}, \frac{\partial \varphi}{\partial y}, \frac{\partial \varphi}{\partial z}, \frac{\partial \varphi}{\partial t} \right) \subset \Omega M,$$

as function of ray-coordinates $(\theta, \phi, t_0, \tau)$. Here τ is the parameter along each ray, $\tau = 0$ on S , and θ, ϕ and t_0 are ray-numbering coordinates. As S is submerged in M , there is a natural mapping, $(\theta, \phi, t_0) \leftrightarrow (x, y, z, t)$, providing the initial conditions for (3.2a). To recover the initial conditions for momentum part (3.2a) of the characteristic system, recall the definition (2.6) of the momentum variables, and let $k_{x0}, k_{y0}, k_{z0}, \omega_0$ be their values on the initial surface S . It then follows that

$$\begin{cases} \frac{\partial \varphi_0}{\partial \theta} = k_{x0} \frac{\partial x}{\partial \theta} + k_{y0} \frac{\partial y}{\partial \theta} + k_{z0} \frac{\partial z}{\partial \theta} - \omega_0 \frac{\partial t}{\partial \theta}, \end{cases} \quad (3.3a)$$

$$\begin{cases} \frac{\partial \varphi_0}{\partial \phi} = k_{x0} \frac{\partial x}{\partial \phi} + k_{y0} \frac{\partial y}{\partial \phi} + k_{z0} \frac{\partial z}{\partial \phi} - \omega_0 \frac{\partial t}{\partial \phi}, \end{cases} \quad (3.3b)$$

$$\begin{cases} \frac{\partial \varphi_0}{\partial t_0} = k_{x0} \frac{\partial x}{\partial t_0} + k_{y0} \frac{\partial y}{\partial t_0} + k_{z0} \frac{\partial z}{\partial t_0} - \omega_0 \frac{\partial t}{\partial t_0}, \end{cases} \quad (3.3c)$$

which together with 3-D Hamiltonian (2.7) evaluated at point $(\theta, \phi, t_0, k_{x0}, k_{y0}, k_{z0}, \omega_0)$ forms a set of four equations for the four unknowns $(k_{x0}, k_{y0}, k_{z0}, \omega_0)$. These are then solved in terms of ray-numbering coordinates (θ, ϕ, t_0) , thus recovering full initial conditions for the characteristic system. Solution of the system (3.2) provides the map

$$(\theta, \phi, t_0, \tau) \mapsto (x, y, z, t, k_x, k_y, k_z, \omega) \in \Omega M,$$

sweeping out the graph of the phase function $\varphi(x, y, z, t)$ in the phase space from the initial surface S . The phase function itself and amplitude coefficients are then reconstructed as described above.

3.2 Monochromatic spherical point source

Let us now derive the initial conditions for a spherical source. Consider a static sphere of a small radius r located at depth $z = z_s$ to be the surface S where the initial conditions for pressure perturbation are set. The surface can be parametrised by the spherical coordinates plus time, (θ, ϕ, t_0) , so that the Cartesian coordinates and time are expressed as

$$\begin{cases} x = x_s + r \cos \theta \sin \phi & (3.4a) \\ y = y_s + r \cos \theta \cos \phi & (3.4b) \\ z = z_s + r \sin \theta & (3.4c) \\ t = t_0, & (3.4d) \end{cases}$$

where $\phi \in [0, 2\pi)$, $\theta \in [-\frac{\pi}{2}, \frac{\pi}{2}]$. Using (3.1-3.3), let $k_{h0}^2 = k_{x0}^2 + k_{y0}^2$ and define $k_{\phi 0}$ so that $k_{x0} = k_{h0} \cos k_{\phi 0}$, $k_{y0} = k_{h0} \sin k_{\phi 0}$, system (3.3) then simplifies to

$$\begin{cases} \frac{\partial \varphi_0}{\partial \theta} = k_{z0} r \cos \theta - k_{h0} r \sin \theta \sin(k_{\phi 0} + \phi), & (3.5a) \\ \frac{\partial \varphi_0}{\partial \phi} = k_{h0} r \cos \theta \cos(k_{\phi 0} + \phi), & (3.5b) \\ \frac{\partial \varphi_0}{\partial t_0} = -\omega_0. & (3.5c) \end{cases}$$

When sound speed and acoustic cut-off frequency depend only on depth, Hamiltonian (2.7) is explicitly independent of x, y and t , so from (3.2a-3.2b) it follows that k_x, k_y and ω are constant along each ray. Therefore, k_h and k_ϕ extended from the above definition throughout the phase space are also constant along rays. When, in addition, the initial phase function φ_0 does not depend on ϕ , e.g. $\partial \varphi_0 / \partial \phi = 0$, it follows that $\cos(k_{\phi 0} + \phi) = 0$, so that via a suitable choice of the x - and y -axis directions $k_{\phi 0} + \phi = \frac{\pi}{2} + 2\pi n$. In this case the system can be reduced to two-dimensions plus time by letting $\phi = \frac{\pi}{2}$, $k_{\phi 0} = 0$ in (3.4), introducing $\hat{x} = x - x_s$, and solving system (2.9), i.e. using (θ, t_0) to find $(\hat{x}, z, t, k_h, k_z, \omega)$. Using symmetry, this solution is then rotated by varying ϕ, k_ϕ to obtain the full three-dimensional field:

$$(\theta, t_0, \tau) \mapsto (\hat{x}, z, t, k_h, k_z, \omega) \hookrightarrow (x, y, z, t, k_x, k_y, k_z, \omega),$$

via

$$x = x_s + \hat{x} \sin \phi, y = y_s + \hat{x} \cos \phi, \quad (3.6a)$$

$$k_x = k_h \sin \phi, k_y = k_h \cos \phi. \quad (3.6b)$$

Point source is approximated by letting r in the definition (3.4) to be infinitely small. A source is spatially homogenous when the initial phase function, φ_0 in (3.1), may depend only on time.

When the dimensionality is reduced, surface S , where initial conditions for the pressure perturbation are set, becomes a circle of

radius, r , located at depth $z = z_s$. The surface is parametrised by coordinates (θ, t_0) with

$$\begin{cases} x = x_s + r \cos \theta & (3.7a) \\ z = z_s + r \sin \theta & (3.7b) \\ t = t_0 & (3.7c) \end{cases}$$

The initial field on this surface is described as

$$\Psi_0 = A_0(\theta, t_0) e^{i\varphi_0(\theta, t_0)}. \quad (3.8)$$

The unknown initial wavenumbers and frequency, $k_{h0} = \partial \varphi_0 / \partial x, k_{z0} = \partial \varphi_0 / \partial z$ and $\omega_0 = -\partial \varphi_0 / \partial t$, are found from the system:

$$\begin{cases} \frac{\partial \varphi_0}{\partial t_0} = k_{h0} \frac{\partial x}{\partial t_0} + k_{z0} \frac{\partial z}{\partial t_0} - \omega_0 \frac{\partial t}{\partial t_0}, & (3.9a) \end{cases}$$

$$\begin{cases} \frac{\partial \varphi_0}{\partial \theta} = k_{h0} \frac{\partial x}{\partial \theta} + k_{z0} \frac{\partial z}{\partial \theta} - \omega_0 \frac{\partial t}{\partial \theta}, & (3.9b) \end{cases}$$

$$\begin{cases} k_{h0}^2 + k_{z0}^2 = \frac{\omega_0^2 - \omega_{ac}^2}{c^2}. & (3.9c) \end{cases}$$

Let us now consider spherical monochromatic homogeneous source of some fixed frequency, ω_f , i.e. $\varphi_0(\theta, t_0) = -\omega_f t_0$. Then from the above $\omega_0 = \omega_f$ and $k_{h0} \sin \theta = k_{z0} \cos \theta$. This implies that in this configuration (see Figure 1) θ can be viewed as ray take-off angle and all rays generated from S are of the same frequency, so frequency subscripts can be dropped. Define

$$k_s^2(z_s, \omega) = \frac{\omega^2 - \omega_{ac}^2}{c^2} \Big|_{z=z_s},$$

then horizontal and vertical wavenumbers can be rewritten as $k_{h0} = k_s \cos \theta$, and $k_{z0} = k_s \sin \theta$. Since Hamiltonian is independent of horizontal coordinate and time, ω and k_h are constant on each ray. Then so is the horizontal phasespeed of a ray,

$$v_{ph}^2 = \frac{\omega^2}{k_h^2} = \frac{c^2}{\cos^2 \theta} \frac{1}{1 - \frac{\omega_{ac}^2}{\omega^2}}.$$

When t_0 is fixed, θ serves as a ray-numbering parameter. Note that by setting $A(\theta, t_0) = 0$, when $\theta < 0$ one can investigate the wavefield generated by rays going down from the source, which would correspond to semi-spheric pump creating pressure at the source. Similarly, taking $A(\theta, t_0) = 0$ for $\theta > 0$ corresponds to the wavefield generated by rays going up to the surface.

4 POLYTROPE

4.1 Individual ray solution

Let us now consider the reduced system in 2 + 1 dimensions with Hamiltonian (2.8a) independent of horizontal coordinate and time. The characteristic equations (2.9) are then considerably simplified:

$$\begin{cases} \frac{dx}{d\tau} = k_h; \frac{dz}{d\tau} = k_z; & (4.1a) \end{cases}$$

$$\begin{cases} \frac{dt}{d\tau} = \frac{\omega}{c^2}; \frac{k_h}{d\tau} = 0; \frac{d\omega}{d\tau} = 0; & (4.1b) \end{cases}$$

$$\begin{cases} k_h^2 + k_z^2 - \frac{\omega^2 - \omega_{ac}^2}{c^2} = 0. & (4.1c) \end{cases}$$

When $k_h = 0$, the corresponding ray propagates purely vertically ($x = \text{const}$). It is easy to see that in terms of the reduction described for spherical source in Section 3.2 this ray travels along the rotation axis.

Consider polytrope model with adiabatic sound-speed and acoustic-cutoff frequency depending on depth only:

$$c^2(z) = \frac{gz}{m}, \quad \omega_{ac}^2(z) = \frac{g(m+2)}{4z}, \quad (4.2)$$

where g is the gravitational constant (the value of $g = 2.67 \times 10^{-4}$ Mm/s² is used in our calculations), and m is the polytrope index. Let us discuss some general properties of such model and eikonal solving associated rays.

A single ray with horizontal wavenumber k_h and frequency ω in this model, in general, will have two turning points, z_u and z_l (upper and lower), determined by the condition $k_z = 0$. In the exceptional case of ray propagating purely vertically, $k_h = 0$, the lower turning point can be viewed as located at infinite depth. Otherwise, using (4.2) one obtains:

$$\begin{aligned} \frac{z^2 k_z^2}{k_h^2} &= -z^2 + \frac{\omega^2 m}{k_h^2 g} z - \frac{m(m+2)}{4k_h^2} \\ &= (z - z_u)(z_l - z) = b^2 - (z - a)^2, \end{aligned} \quad (4.3)$$

where z_u, z_l are the upper and lower turning points and $a(k_h, \omega) = (z_u + z_l)/2$, $b(k_h, \omega) = (z_l - z_u)/2$. These can also be written as

$$a(k_h, \omega) = \frac{1}{2} \frac{\omega^2 m}{k_h^2 g}, \quad b(k_h, \omega) = \sqrt{a^2(k_h, \omega) - \frac{m(m+2)}{4k_h^2}}.$$

Note that the upper and lower turning points coincide when $b = 0$.

Furthermore, in this model the wave-vector length, $k^2 = (\omega^2 - \omega_{ac}^2)/c^2$, viewed as function of z only, has a maximum at $z_E = g(m+2)/2\omega^2$ determined by $\omega_{ac}^2(z_E) = \omega^2/2$. This value is important due to the following more general statement:

Proposition 1. With Hamiltonian H in (2.8a) independent of x and t , every ray solving (2.9) that has two distinct turning point depths, z_u and z_l , will pass through at least one point with $z = z_E$, where z_E is such that

$$\left. \frac{\partial}{\partial z} \left(\frac{\omega^2 - \omega_{ac}^2}{c^2} \right) \right|_{z=z_E} = 0.$$

Indeed, according to (2.9),

$$\frac{dk_z}{d\tau} = -\frac{\partial H}{\partial z} = \frac{\partial}{\partial z} \left(\frac{\omega^2 - \omega_{ac}^2}{c^2} \right)$$

. But this is the rate of change of vertical wavenumber along the ray, and since $k_z(\tau)$ is smooth and becomes zero at turning points, it will have an extremum between them.

Corollary 1. If for a given frequency there exists a unique "partition depth" $z = z_E$ such that

$$\left. \frac{\partial H}{\partial z} \right|_{z=z_E} = 0,$$

then for all rays with distinct upper and lower turning points the following inequalities are true: $z_u < z_E, z_l > z_E$. Ray starting at depth z_E with

$$k_h^2 = \left. \frac{\omega^2 - \omega_{ac}^2}{c^2} \right|_{z=z_E}$$

will propagate horizontally.

In the polytrope model, b becomes zero only when ray is initialised at depth $z_E(\omega)$ with $k_h = \omega^2 m / 2gz_E$. It follows that under these conditions $a = z_E$.

Since $\omega/c^2 \neq 0$ in the domain of interest, $z > 0$, one can rewrite system (4.1) using group travel time, t_g , as the parameter along the ray, with $t = t_g + t_0$, to obtain

$$\begin{cases} \frac{dx}{dt_g} = \frac{gz}{\omega m} k_h, & \frac{dz}{dt_g} = \frac{gz}{\omega m} k_z \end{cases} \quad (4.4a)$$

$$\begin{cases} \frac{d\omega}{dt_g} = 0, & \frac{dk_h}{dt_g} = 0, \end{cases} \quad (4.4b)$$

$$\frac{z^2 k_z^2}{k_h^2} = b^2 - (z - a)^2 \quad (4.4c)$$

Therefore when $b \neq 0$,

$$\sin^{-1} \left(\frac{z - a}{b} \right) = \frac{k_h g}{\omega m} t_g + C_z,$$

hence,

$$z = a + b \sin \alpha, \quad (4.5a)$$

$$x = \frac{1}{2} \frac{\omega}{k_h} t_g - b \cos \alpha + C_x, \quad (4.5b)$$

where $\alpha = t_g k_h g / \omega m + C_z$ and integration constants C_z and C_x are determined from the initial conditions. For $b = 0$ it is easily checked that $z = z_E = a, x = \omega t_g / 2k_h + C_x$, i.e. (4.5b) still holds. In the case when $k_h = 0$, $x = \text{const}$, $z = gt_g^2 / 4m \pm C_z t_g \sqrt{g/m} + C_z^2$, where the choice of sign depends on the direction of the ray propagation and C_z is determined from the initial conditions.

Using group travel time as a parameter along the ray leads to a following interpretation. Let (ξ, t_0) be the coordinates on the initial surface with the field described there as

$$\Psi_0 = A_0^0(\xi, t_0) e^{i\varphi_0(\xi, t_0)},$$

such that $A_0^0 = 0$ when $t_0 < 0$. Then from (2.12) it follows that $A_0(\xi, t_0, t_g) = 0$ along the ray when $t = t_0 + t_g < t_g$. Hence, group travel time is the time it takes for the initial perturbation to travel to a point along the ray and surfaces $t_g = \text{const}$ represent wavefront snapshots at a particular time (Kravtsov & Orlov 1990).

Using the monochromatic spherical source initial conditions (3.7-3.8) with $x_s = 0$ the ray system can be solved in terms of co-ordinates (θ, t_0, t_g) as shown in Appendix A. Given source depth, z_s , the solution is written in terms of take-off angle, θ , and group travel time t_g . The group travel time is expressed via a parameter $\alpha(\theta, t_g)$ and its initial value $\alpha_0(\theta, z_s)$. Solution for α_0 is given in (A4), which reveals the importance of the source position relative to the turning point partition depth, z_E . Formulas (A1a-A1e) together with the system (A5) provide the immersion of the phase function graph into phase space: $(\theta, t_0, t_g) \hookrightarrow \Omega M$. Formulas (A1a-A1d) themselves represent the projection of such map to M : $(\theta, t_0, t_g) \mapsto (x, z, t)$. Due to the simple translational relationship (A1c) between the group travel time and time and initial time variables, when considering eikonal solution one is justified in simply fixing t_0 . Then for $\theta = \text{const}$, (A1a-A1d) provide parametric ray solution as a function of t_g , while taking $t_g = \text{const}$ gives geometric wavefront at the time, $t = t_g + t_0$, as function of take-off angle θ .

Examples of the solutions in terms of ray and wavefront propagation for monochromatic spherical sources placed at two different depths are presented in Figure 2. In both cases, the polytrope index is set as $\frac{3}{2}, t_0 = 0$, and source frequency, $\nu = \omega/2\pi$, is 6.5 mHz. Each panel represents a spatial snapshot of the eikonal system at a particular time which is given in the panel title. The wavefront is plotted as thick red curve, selected ray paths up to the time indicated are plotted in black. The left column corresponds

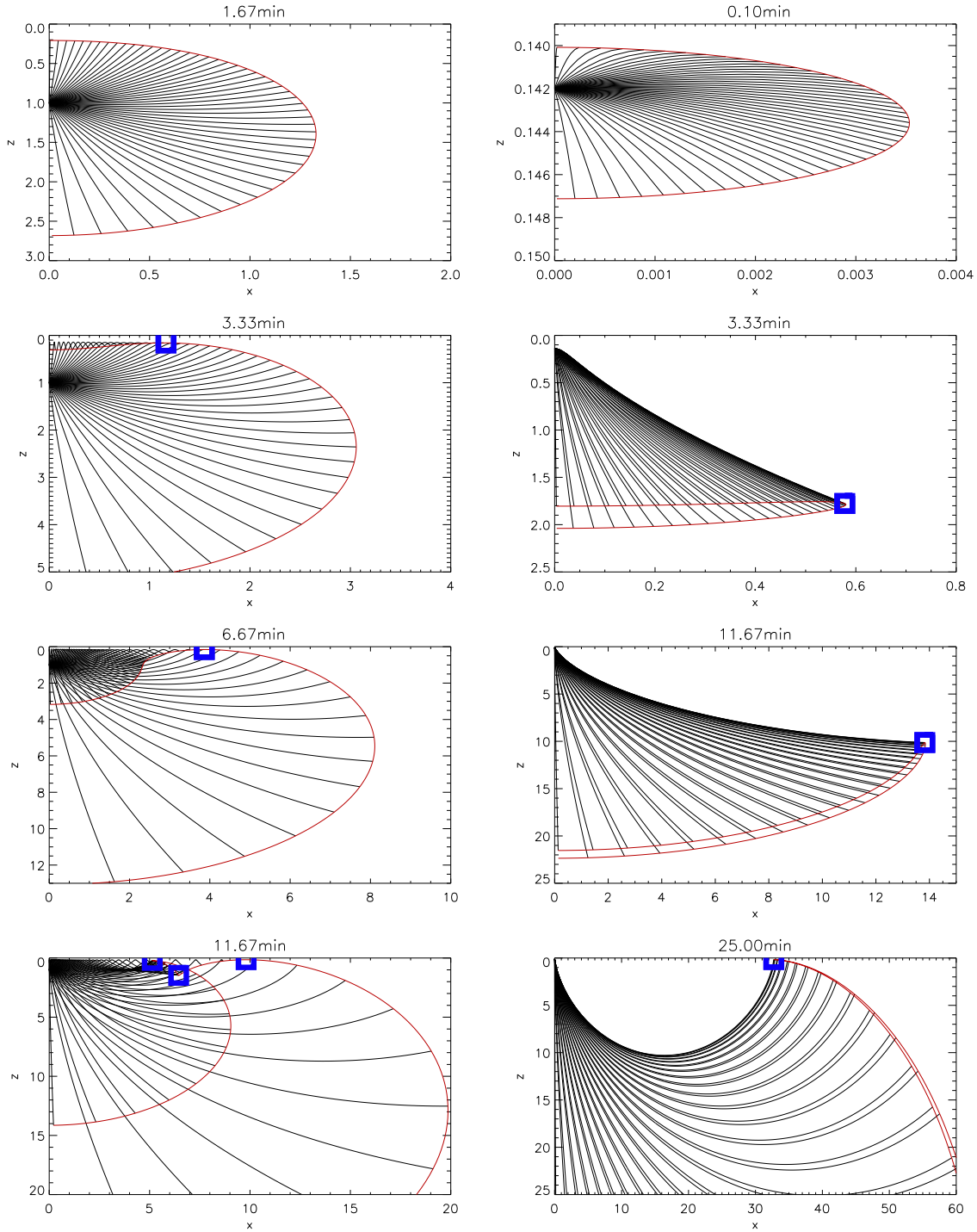


Figure 2. Acoustic wavefront at different times generated by monochromatic point source with frequency $\nu = 6.5$ mHz with $z_s = 1$ Mm (*left*) and $z_s = .142$ Mm (*right*). Rays start at $t_0 = 0$, slice times are given in plot titles, geometric wavefront is plotted in red, with selected time-limited rays in black. Caustic points are marked by blue squares. The polytrope index is taken as $m = \frac{3}{2}$. The surface is located at $z = 0$. Note that the right column corresponds to the case when the source is placed in the region where variability of the model is high, so that the eikonal approximation becomes invalid. Indeed there are reasons to think that such a solution does not represent a physically realistic scenario (C. Lindsey - private communication). See Section 5.1.1 for discussion of applicability.

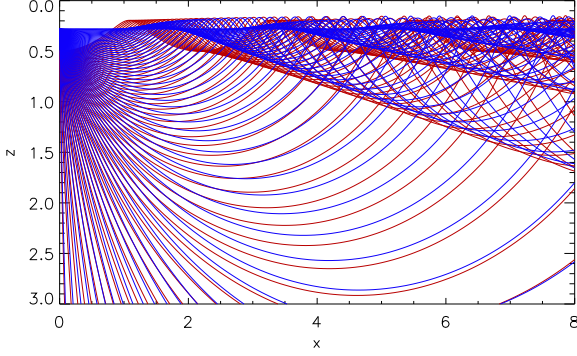


Figure 3. Downward propagating rays with $\nu = 6.5$ mHz, $m = \frac{3}{2}$ for point-sources at depths of 1 Mm (blue) and 2 Mm (red). Envelopes of the ray families representing the caustics are clearly seen.

to the case $z_s = 1$ Mm $> z_E$, right column shows snapshots for $z_s = 0.142$ Mm $< z_E$. After simultaneously leaving the source, rays propagate up ($\theta < 0$) and down ($\theta > 0$) from the source sweeping out the generated wavefront. Near the surface, at the upper turning points rays reflect back to the interior due to acoustic-cutoff frequency increase. In the interior the rays are reflected back to the surface at lower turning points. As different rays reach turning points at different times, the wavefront gets deformed. This is discussed in the next Section. When source is located below the partition depth z_E (left column), wavefront reaches the surface with the rays going up from the source and then propagates radially outward in the near-surface layers with the second bounce surface manifestation appearing later. When source is located above z_E , the situation is different: after initial surface bounce for rays going up from the source, the reflected wavefront goes below the surface mirroring the behaviour of the rays going down, before reappearing some distance away from the source and then travelling radially outward in the near surface layers. This is further discussed in Section 4.3.

4.2 Caustics

Figure 3 shows two families of rays generated by semi-spherical point sources located at 1 and 2 Mm depths. In both cases, the downward pump scenario² is represented, i.e. $A_0^0(\theta, t_0) = 0$ when ($\theta \geq 0$), so only downward propagating rays are plotted. It can be seen that near the upper and the consecutive lower turning points the density of the projected onto M characteristic curves (i.e. rays) increases with ray families becoming enveloped by “caustics”. Caustics are defined as surfaces where the Jacobian of the coordinate transform from ray to Cartesian coordinates becomes zero. This implies that at such points the mapping is not unique, i.e. two or more rays pass through the same point in (x, z, t) space. It can be checked that, under the initial conditions considered here, this is equivalent to the wave-vector being tangent to the wavefront. As wavefront propagates in the direction of its tangent and rays travel in the direction of the wave-vector, it follows that such points locally envelop the wavefront and ray-paths. Caustics are often, though not always, associated with the singularities of the

generated wavefronts such as cusps. See (Kravtsov & Orlov 1990; Kravtsov & Orlov 1993) and references therein for more details.

For $\theta \in (-\frac{\pi}{2}, \frac{\pi}{2})$, analytical expression of the Jacobian of the transform from ray-to-Cartesian coordinates is derived in Appendix A2 (see (A10)). Evaluating $J(\theta, \alpha)$ at lower turning points, $\alpha = \frac{\pi}{2} + 2n\pi$, gives $J(\theta, \frac{\pi}{2} + 2n\pi) = -z_l^3 \tan \theta / b$, and at the upper: $J(\theta, -\frac{\pi}{2} + 2n\pi) = z_u^3 \tan \theta / b$. It follows then that the turning points are on caustics only when $\theta = 0$. Moreover,

$$J(0, \alpha) = bz_s \cos \alpha \left(1 - \frac{\xi}{2} \frac{\partial \alpha_0}{\partial \theta}(0) \right) = -2b \frac{z_s}{\xi - 2} \cos \alpha,$$

so that the ray with $\theta = 0$ touches caustics only at its turning points. In particular, this means that the initial value of the Jacobian is zero, which according to (2.12) indicates that in zero-order approximation the amplitude of the wave-field will be zero along the ray. When take-off angle is non-zero, the fact that the Jacobian along the ray takes different signs at upper and lower turning points suggests that there is at least one caustic point situated in between.

The caustic points, computed numerically using (A10), at given times are plotted as blue squares in Figure 2. In both cases caustics are formed after rays went through the turning points. When $z_s < z_E$, right column, the first caustic is formed at the interface of the downward propagating front and the reflected from the surface following front. Once this caustic comes back to the surface (the bottom plot), it then propagates near the surface away from the source. In the case when $z_s > z_E$, left column, the first caustic point is formed near the surface when the ray with $\theta = 0$ passes through the upper turning point. The point then travels radially in the near-surface layers away from the source. The bottom image shows the appearance of the next set of caustic points, one of which is again located near the surface and is associated with the second bounce waves at the surface. The others correspond to wavefront cusp formed near lower turning points. A close-up example of the formation of caustics associated with the wave-front cusp is shown in the Figure 4.

In Figure 5 locations of the caustics and turning points are compared. It can be seen that the lower caustics are associated with lower turning points for second and further bounces. These caustics are quite close to the locations of the turning point, though not exact except for $\theta = 0$. The caustics formed near the surface are very close to rays’ upper turning points. Moreover, near surface caustics are generally quite basic, e.g. not associated with wavefront singularities, and are formed when only two rays (one after being reflected and another coming up to its reflection point) intersect.

The results presented in this Section agree well with the analysis of the numerical simulation of acoustic wave propagation in the solar interior (Shelyag et al. 2009). Further analysis is needed to rigorously determine types of the caustics generated by a spherical point source and hence describe acoustic field behaviour in their neighbourhood.

4.3 Wavefield at the surface

As no direct observations of the Sun below the photosphere are available, the surface manifestation would be a primary observable for any acoustic wave-field generated in the interior or near the surface. Let $x_{surf}(\theta|\omega, z_s) = x_{surf}(\theta)$ denote the horizontal distance from the source to the first appearance of the ray on the surface, i.e. its first upper turning point. As shown in Appendix A1, upper turning points correspond to $\alpha = -\frac{\pi}{2} + 2\pi n$, so the first such point away from the source depends on the choice of initial value, α_0 .

² see the last paragraph of Section 3.2

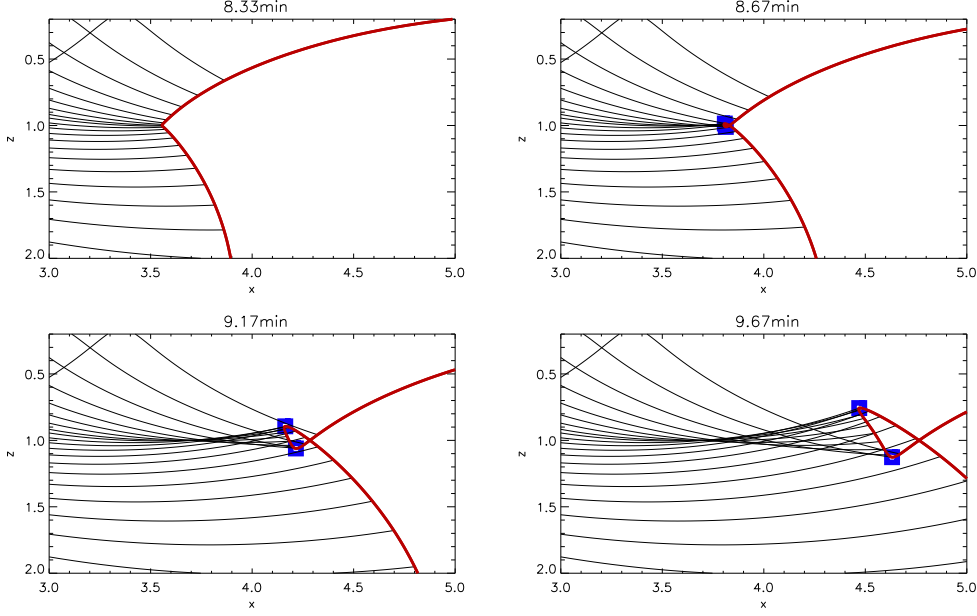


Figure 4. Formation of the wavefront singularity and caustics near lower turning points, for $z_s = 1$ Mm, $\nu = 6.5$ mHz. The caustic is formed when “up” rays after being reflected near surface, intersect “down” rays travelling up to the surface after passing the lower turning point.

When source is placed at or below z_E , $z_s \geq z_E$, the situation is straight forward with $\alpha_0(\theta) \in (-\frac{\pi}{2}, \frac{3\pi}{2})$ for $\theta \in (-\frac{\pi}{2}, \frac{\pi}{2})$, so that the first upper turning point along every ray corresponds to $\alpha = \frac{3}{2}\pi$. Then

$$x_{surf}(\theta) = z_s \frac{\xi}{2 \cos^2 \theta} \left(\frac{3}{2}\pi - \alpha_0 \right) + z_s \tan \theta, \quad (4.6)$$

where

$$\xi = \frac{\omega^2}{\omega^2 - \omega_{ac}^2} \Big|_{z=z_s}$$

(see Appendix A1 for more details). The corresponding group travel time, $t_{g,surf}$, the time it takes for the perturbation to travel along the ray from the source to ray’s first upper turning point, is given as

$$t_{g,surf} = \frac{\omega m}{k_{hg}} \left(\frac{3}{2}\pi - \alpha_0 \right). \quad (4.7)$$

When source is placed above z_E , i.e. $z_s < z_E$, α_0 is less or equal to $-\frac{\pi}{2}$ when θ is negative (rays going up from the source), and greater than or equal to $-\frac{\pi}{2}$ when θ is positive. Thus,

$$x_{surf}(\theta) = \begin{cases} z_s \left(\frac{1}{2} \frac{\xi}{\cos^2 \theta} \left(-\frac{\pi}{2} - \alpha_0 \right) + \tan \theta \right), & \theta < 0; \\ z_s \left(\frac{1}{2} \frac{\xi}{\cos^2 \theta} \left(\frac{3}{2}\pi - \alpha_0 \right) + \tan \theta \right), & \theta \geq 0, \end{cases}$$

with corresponding group travel times:

$$t_{g,surf}(\theta) = \begin{cases} \frac{\omega m}{k_{hg}} \left(-\frac{1}{2}\pi - \alpha_0 \right), & \theta < 0; \\ \frac{\omega m}{k_{hg}} \left(\frac{3}{2}\pi - \alpha_0 \right), & \theta \geq 0. \end{cases}$$

Due to the symmetry of the initial conditions, the surface ripples will propagate circularly away from the source, following the time-distance relationship defined above using the take-off angle as parameter. Comparing these time-distance relations with the one for skip-distance, $\Delta = t_{\Delta}^2 g / 4\pi m$ (see Appendix A1 for details), it is useful to separately consider rays going up and down from the source. The rays going up reach their upper turning point first and

reflect back to the surface. After that the first surface ripple is defined by the rays leaving the source away from the surface and then reflected back.

- when $z_s \geq z_E$, after the up-propagating rays are reflected from the surface, the time-distance curve is similar to the skip-distance relationship with times slightly scaled, since the rays do not travel the whole skip-distance (distance between surface bounces). This scaling/difference depends on the source frequency and depth, via parameter ξ . See left column of Figure 2 for an example of such source.

- when $z_s < z_E$, after the initial surface bounce of “up” ($\theta < 0$) rays, the time-distance curve is even closer to the skip-distance relationship, with wavefront from down rays slightly pre-ceding the skip-distance arrival time, while the up-ray wavefront which was initially reflected from the surface near the source, arriving slightly later due to the time it takes for the ray to travel from the source to the surface. See right column of Figure 2 for an example of such source.

5 DISCUSSION AND APPLICATIONS TO THE SUN

Before moving to the discussion of the applications of this method to the Sun, let us briefly review existing observations of the acoustic wave-fronts. While acoustic oscillations in the Sun have been extensively studied via global and local helioseismology, our understanding of the nature of their excitation remains relatively sketchy with stochastic turbulent convection generally considered to be the main mechanism responsible. There is, however, a recently discovered sunquake phenomena that provides us with observational examples of locally generated acoustic fields. Sunquakes, which are relatively rare events (please see Donea 2011, for discussion on detectability), take place in active regions during flares, when the flare induced changes in sunspot penumbra under the right circumstances generate acoustic waves. These waves can be seen in

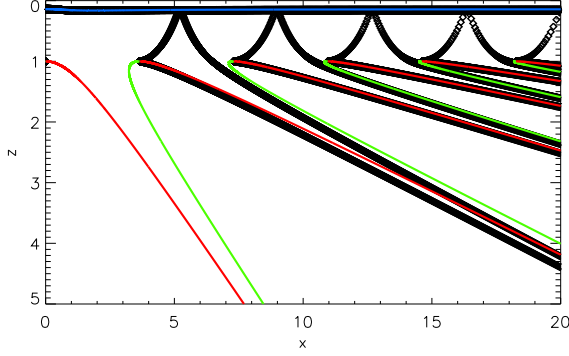


Figure 5. Caustics and turning points: projection of caustics onto spatial plane are thick black lines. Lower turning points of rays going down from the source are drawn in red, with lower turning points for rays going up from the source drawn in green. Upper turning points are in purple.

photospheric Dopplergram observations as circular shaped surface ripples (Kosovichev 2006; Moradi et al. 2007; Kosovichev 2011) accelerating away from the source region. However, due to background oscillations, such ripples are often difficult to distinguish, so helioseismic methods such as time-distance diagram analysis and acoustic holography are usually applied to suitably processed series of line of sight velocity observations for quake detection.

Time-distance method (Kosovichev & Zharkova 1998; Kosovichev 2007, 2011; Zharkov et al. 2012) provides direct observational evidence of generated acoustic waves by integrating the signal over circles or arcs centred at the source for every observation in the time-series, thus producing a 2-D diagram displaying the field dependence on time and distance from the source. In such diagrams quake events have a clear signature in the form of a discernible time-distance ridge. It is the close agreement between the detected ridges and the theoretical travel-time skip-distance relation that provided the conclusive proof of sunquakes acoustic nature. On the other hand, the acoustic egression measurements (Donea et al. 1999; Donea & Lindsey 2005; Lindsey & Donea 2008; Matthews et al. 2011) are based on theoretical modelling of acoustic waves propagating from a point source and provide a proxy measurement of acoustic energy emitted at a location at given time, thus producing a map of acoustic sources and sinks. Quake signatures in egression power maps are normally represented by a compact kernel or kernels of enhanced emission surrounded by the acoustically absorbing sunspot interior (see Zharkov et al. (2011b, 2012) for discussion and comparison of the two methods).

Both methods were originally based on the assumption of photospheric manifestation of a flare generated acoustic field in the form of circular shaped ripples propagating away from the source. However, considerable anisotropy in the acoustic amplitude of the ripples from the vantage of the sources has been observed for most quakes (Kosovichev 2006; Moradi et al. 2007; Donea 2011) with acoustic emission stronger in some directions than others and ripples changing shape becoming elliptical.³ In egression power maps such anisotropy is represented by “stacked

acoustic kernels”, where two or three narrow kernels are stacked together. Donea et al. (1999); Donea & Lindsey (2005) suggested that this could be the result of interference caused by the rapid motion of the source, roughly in the direction along which the kernels are stacked. This was supported by observations of apparent rapid photospheric movements at the quake locations. Donea & Lindsey (2005) found that for 2003 October 28 and 29 quakes the motion of the HXR sources was indeed aligned accordingly with egression power stacks. This was further confirmed for 2002 July 23 flare by Kosovichev (2007) using HXR and Doppler data, where via data analysis and modelling the author estimated the speed of the seismic source to be supersonic⁴ around $20 - 25 \text{ km s}^{-1}$. More recently, Kosovichev (2011) used time-distance diagram analysis to detect a supersonic movement of one of the seismic sources produced by 2011 February 15 flare, with speed around $15 - 17 \text{ km s}^{-1}$. Supersonic motions of around $14 - 22 \text{ km s}^{-1}$ have also been detected for this flare’s second seismic source in Zharkov et al. (2012). In the recent review Donea (2011) notes that the maximum amplitude of the ripples emanating from a moving source is generally along the axis of the source, displaced from the source location in the direction of the motion.

Both helioseismic methods have shown very local spatial nature of the seismic sources validating the point source assumption. However, there is no current consensus in regard to the physical mechanism and processes behind the quake excitation. Backwarming heating, hydrodynamic shocks, particle precipitation and Lorentz force are the main scenarios currently considered and debated as those capable of producing flare acoustic response (see Donea (2011) and references therein for more details). Due to the lack of our current understanding of excitation, little is known about the depth of the source, but it is generally assumed to be near the photosphere since various modelling methods show only a small fraction of the energy initially invested in the shock penetrate into the photosphere.

5.1 Stationary monochromatic source

Back to the model considered in Sections 3-4, it is clear that non-evanescent acoustic waves are present in the model if and only if $k^2 \geq 0$. Then the first condition on monochromatic source being able to generate acoustic wavefield is $\omega^2 > \omega_{ac}^2(z_s)$. Let $z_{cut}(\omega)$ denote the point such that $\omega_{ac}^2(z_{cut}) = \omega^2$. Furthermore, as shown in Section 4.1, the presence of a unique extrema in the $k^2(z) = (\omega^2 - \omega_{ac}^2)/c^2$ warrants the existence of the (upper and lower) turning point partition depth z_E . When such a partition depth exists, placing a source above it (but with $\omega > \omega_{ac}(z_s)$) will create a gap in ripples seen at the surface. Indeed, using the fact that for a fixed frequency the skip-distance for a particular ray is a function of its horizontal wavespeed, one can evaluate

$$k_h^2 \leq \frac{\omega^2 - \omega_{ac}^2}{c^2} \Big|_{z=z_s} = k^2(z_s),$$

therefore $v_{ph}^2 \geq c^2 \omega^2 / (\omega^2 - \omega_{ac}^2)$. As ω_{ac}^2 grows near the surface, z approaches z_{cut} and the phase speed grows infinitely large. As upper turning depths of the rays are greater than z_E , and since near upper turning points ray propagate nearly vertically, it is clear that rays going up from point source will not travel far from the source horizontally before being turned back down into the interior. For

³ for example, using directional time-distance diagrams Kosovichev (2011) has reported strong travel-time anisotropy in different arcs of the wave-front generated by the strongest seismic source of 2011 February 15 flare

⁴ in the quiet Sun adiabatic soundspeed at the photospheric level is estimated around $7 - 8 \text{ km s}^{-1}$ in the quiet Sun

rays going down from the source the horizontal distance from the source to its first appearance at the surface will be slightly shorter than its skip-distance, so that the first appearance at the surface will be approximately at $\Delta(\min v_{ph}^2)$. Thus, for example, for polytrope model considered in Section 4.1, taking $m = \frac{3}{2}$, at $z = 122$ km only waves with frequency $\nu = \omega/2\pi \geq 7$ mHz can be generated. Moreover, given z_s , if ω is close to the value of the $\omega_{ac}(z_s)$, the distance where generated waves surface away from the source can grow very large due to the fact that $k_h^2 \leq (\omega^2 - \omega_{ac}^2)/c^2$.

The assumption of a unique extrema for $k^2(z)$ doesn't hold in the case of Model C (Christensen-Dalsgaard et al. 1996), a widely used and thoroughly tested in helioseismology model of non-magnetic solar interior. This is due to multiple peaks in acoustic cut-off frequency present near the surface (see bottom panel of Figure 6). This effect, however, is thought to be numeric in nature (see Schunker & Cally 2006, for example) and other models such as isothermal cut-off frequency, $c^2/4H_p^2$, are often used in the acoustic oscillation studies in order to ensure smooth variation. It can be checked that in the isothermal case such an extrema exists, and corresponds to a maximum that appears to be unique below the surface for frequencies of up to ≈ 7 mHz.

Adiabatic sound speed and acoustic cut-off frequency estimated from this model are presented in Figure 6. It is seen from Figure 6, where sound speed and acoustic cut-off frequency estimated from the model are plotted, that in the layers where ω_{ac} is large c is of the order of 7-8 kilometres per second. Note that in the Sun high frequency rays will not necessarily have an upper turning point, escaping into the outer layers of solar atmosphere.

5.1.1 Applicability of the method

Before going further, let us note some considerable limitations of the model and solution using the shallow source considered in the earlier sections as an example. Stationary monochromatic source solution suggests that when the source is placed close to the surface the generated wavefront can surface some distance away from the source (right column, Figure 2). If this were to be applicable to sunquakes, it would imply that the detection of such events may require a field of view larger than currently used. And even then the detectability of such waves via local helioseismic methods might be difficult due to reduced wave amplitude at large distances from the source.

However, clearly the model used here is too basic to expect a realistic representation of the physical phenomena. Apart from the glaring lack of magnetic field which we know is present at sunquake locations, the Brunt Vassala frequency is also zero, $N^2 = 0$ in (2.1). Employing ray-mechanical formalism Barnes & Cally (2001) have shown the importance of Brunt Vassala term for waves near the acoustic cut-off boundary.

There are also limitations associated with the solution itself. Firstly, by applying the condition $k_z^2 \geq 0$ and thus rejecting complex valued wave-numbers, the phenomena such as jacket modes is omitted, whereas those are needed to form a complete set of wave-equation solutions (Bogdan & Cally 1995). This can possibly be addressed via extending the solution to complex rays, and for example considering the signal from downward propagating evanescent modes, i.e. with imaginary k_z , and evaluating if and how it can transform into pure acoustic rays at larger depths.

Furthermore, the dispersion relation, corresponding Hamiltonian and rays associated with initial conditions are derived from the eikonal equation (2.5a). The actual wave-field is then reconstructed by solving the set of transport equations (2.5b, 2.5c, ...) and postu-

lating or establishing that the resulting series (2.4) are asymptotic to the exact solution. Under certain conditions such as slow-variability of the model (Kravtsov & Orlov 1990; Gough 2007), an "almost" plane-wave (or eikonal) approximation can be justified, where the resulting field is approximated via its zero-order amplitude. The usual interpretation of rays as paths along which the energy propagates is based on such an approximation. This is clearly not the case for the shallow source where, due to the properties of acoustic cut-off frequency, model variability becomes high. As sufficient conditions for the "almost" plane wave approximation are clearly not met, this needs further investigation, e.g. solving higher order transport equations or approaching the problem via different methods. In fact, based on more realistic wave modelling, there are reasons to think that physical situation is different. (C.Lindsey - private communication).

Thus, the properties of the eikonal solution discussed here and in the following section should be considered as hypothetical, possibly posing questions about real physical scenarios and applicability of the geometric asymptotics method.

5.2 Moving source

Let us now consider a moving source. This is achieved by going back to (3.4) and letting the source coordinates (x_s, y_s, z_s) depend on time t_0 . It is clear that the symmetry is broken unless the source moves along the axis of rotation, so the three-dimensional equations are considered. When solving the system (3.3), use the stationary source case outlined in Section 3.2. As $\partial\varphi_0/\partial\theta$ and $\partial\varphi_0/\partial\phi$ are actually the same, k_{h0} and $k_{\phi 0}$ are defined in the similar manner, and with equations (3.5a-3.5b), it also follows that $\cos(k_{\phi 0} + \phi) = 0$. It is only the frequency definition (3.5c) that is affected by source movement:

$$\frac{\partial\varphi_0}{\partial t_0} = \mathbf{k}_0 \cdot \mathbf{v} - \omega_0, \quad \text{where } \mathbf{v} = \frac{d\mathbf{x}_s}{dt_0},$$

represents source velocity. Similar to Section 3.2 let the initial phase in the definition (3.8) be monochromatic and homogenous, i.e. $\varphi_0 = -\omega_f t_0$. Then, the initial ray frequency is given as

$$\omega_0 = \omega_f + \mathbf{k}_0 \cdot \mathbf{v}. \quad (5.1)$$

Hence, in this case, the source frequency is modified depending on the wave-vector: ray frequency which is constant along each ray varies from one ray to another according to $\omega_0 = \omega_f + k_0 v \cos \gamma$, where γ is the angle between the wave vector and source velocity. The frequency increases along the vector of the source movement, and decreases when the wave-vector points in the opposite direction.

Similar to stationary source (see Section 3.2), it follows from the first two equations in (3.3) that $k_h = k_0 \cos \theta$, $k_{z0} = k_0 \sin \theta$, where $k_0^2 = (\omega_0^2 - \omega_{ac}^2)/c^2$. Then use the dispersion relation $H = 0$, where Hamiltonian H is defined in (2.7), to find k_0 . Substituting (5.1) into the last expression, the following quadratic equation with respect to k_0 is obtained:

$$k_0^2(u^2 - 1) + 2\frac{\omega_f}{c}uk_0 + \frac{\omega_f^2 - \omega_{ac}^2}{c^2} = 0, \quad (5.2)$$

where $u = v \cos(\gamma/c)$. Consider the case when, as before, the source with frequency greater than the acoustic cut-off value, $\omega_f \geq \omega_{ac}(z_s(t_0))$ moves with subsonic speed, $v < c \implies u^2 < 1$. The solution is

$$k_{0\pm} = \frac{1}{c} \frac{\omega_f u \pm \sqrt{D}}{1 - u^2} \implies \omega_{0\pm} = \frac{1}{1 - u^2} (\omega_f \pm u\sqrt{D}),$$

where $D = \omega_f^2 - \omega_{ac}^2 + \omega_{ac}^2 u^2$. Clearly, under our assumptions $D > 0$. Since k_0 is defined as length of the wave-vector, we are looking for positively valued roots only, which leaves only k_{0+} and ω_{0+} .

To visualise the nature of the angle γ let us now define an appropriate coordinate frame. Assume that at the time t_0 the source is located at $x_s(t_0) = y_s(t_0) = 0$. Since there is freedom in selecting the direction of x - and y - axes, choose coordinate axes so that the source moves in the direction of y -axis, i.e. $\mathbf{v} = (v_x, 0, v_z)$. In spherical coordinates, (r, θ, ϕ) , defined for the source, $\mathbf{v} = (v, \lambda, 0)$, where λ is the angle between the velocity vector and xy -plane. Then, using the spherical law of cosines, for any wave-vector $\mathbf{k}_0 = (k_0, \theta, \phi)$ we have

$$\cos \gamma = \sin \theta \sin \lambda + \cos \theta \cos \lambda \cos \phi. \quad (5.3)$$

Note that apart from the assumption of dependence on depth only all of the above does not depend on the model for the sound speed and acoustic cut-off.

In the polytrope model the ray solution derived in the Appendix, (A1a-A1e) together with (A4) and (A5), holds for individual rays. However, the generated wave-field will have a more complex dependence on the parameter t_0 , due to the source movement. E.g. at moment t_0 source produces a family rays governed by the above equations, then at moment $t_0 + \delta t$ the source will have moved producing another family of rays. This will be investigated in future publication.

5.3 Supersonic source

While the wave-fields generated by a monochromatic point source have some of the properties associated with solar quakes, one of the main limitations of the considerations above is the assumption of source frequency. Even for observed high frequency⁵ waves generated by flares, the period is still of the order of couple of minutes. At the same time, the photospheric changes observed at the quake locations happen on a much shorter scale (Zharkova & Zharkov 2007; Kosovichev 2007, 2011; Zharkov et al. 2011a, 2012).

It is instructive to consider a non-harmonic source, i.e. $\varphi_0(\theta, \phi, t_0) = 0$. This corresponds to the wave-field on initial surface simply written as $\Psi_0 = A_0(\theta, \phi, t_0)$, meaning that the pressure perturbation, $\rho^{\frac{1}{2}} \delta p$, is varying slowly on the initial surface. As in previous Section 5.2, $\partial \varphi_0 / \partial \theta = 0$, $k_{z0} = k_{h0} \tan \theta$, system (3.3) leads to the following solution:

$$\begin{cases} k_0^2 = \frac{\omega_{ac}^2}{v^2 \cos^2 \gamma - c^2}, & (5.4a) \\ \omega_0 = \mathbf{k}_0 \cdot \mathbf{v} = k_0 v \cos \gamma, & (5.4b) \\ k_{h0} = k_0 \cos \theta, \quad k_{z0} = k_0 \sin \theta, & (5.4c) \end{cases}$$

where \mathbf{k}_0 is the wavevector, \mathbf{v} is source velocity, $v = |\mathbf{v}|$, and γ is the angle between the two vectors. From the above it follows that non-evanescent acoustic waves ($k_0^2 > 0$) are generated if and only if the source moves with supersonic speed $v^2 > c^2$. Moreover, let us rewrite (5.4b) as

$$\omega_0 = \omega_{ac} \frac{\cos \gamma}{\sqrt{\cos^2 \gamma - \frac{c^2}{v^2}}}, \quad (5.5)$$

where the square root is always taken with plus sign due to (5.4a) and the fact that $k_0 > 0$ by definition. Again, it is clear that while

the frequency is constant on each individual ray, it will vary from ray to ray as parameterised by θ, ϕ and t_0 . It is also evident that in this case ω_0 is always greater than the value of ω_{ac} at the source depth, going to infinity as $\cos^2 \gamma \rightarrow c^2/v^2 < 1$. In addition, $\omega_0 \geq \omega_{min} = \omega_{ac} v / (\sqrt{v^2 - c^2})$. Note that when $\cos \gamma$ is negative ω_0 becomes negative, so waves will only be generated in the direction of the source movement. Moreover, given the (5.3), the condition

$$\cos^2 \gamma > \frac{c^2}{v^2} \quad (5.6)$$

ensures that rays are generated for only a relatively narrow range of values of θ and ϕ , essentially forming a cone around the velocity vector \mathbf{v} . The horizontal phase speed at the source does not depend on source depth: $v_{ph} = \omega_0 / k_{h0} = v \cos \gamma / \cos \theta$.

Again, note that apart from the assumption of dependence on depth only all considerations in this section are independent of the model of the media where the waves propagate and rely only the dispersion relation as well as spatial geometry of the problem. Also, note that this solution is only possible when $\omega_{ac} > 0$.

5.4 Comparison with sunquakes

As quake observations and modelling suggest the source is located near surface, let us assume that the source moves in the upper ranges of solar interior, so that for generated frequencies $z_s < z_E$, i.e. the source is located near upper turning points. Then, for each generated ray, the horizontal distance from the source approximately equals to the skip-distance, $\Delta(k_h, \omega)$. On the other hand, the skip-distance is essentially a function of horizontal phase speed of the ray with lower phase-speed values corresponding to smaller distances. The relationship is exact for polytrope and other theoretical models (see Christensen-Dalsgaard 2003) and has been observationally validated by the time-distance helioseismology and acoustic holography.

Let us consider a source propagating with velocity v vertically downward, i.e. $\lambda = \frac{\pi}{2}$ (see (5.3)). Then $\cos \gamma = \sin \theta$, and as only downward propagating rays are generated, the first appearance of the generated wavefront on the surface corresponds to the minimum value of $v_{ph} = v \tan \theta$. Then for $\theta \in [0, \frac{\pi}{2}]$ the minimum horizontal phase speed will be achieved at the lowest value of θ . Using (5.6) one obtains

$$\min v_{ph} = \frac{vc}{\sqrt{v^2 - c^2}}, \quad (5.7)$$

where expression on the right hand side is evaluated at $z = z_s$. However, frequency of the rays travelling near such phase speed will be approaching infinity due to (5.5). Hence if observations are made at certain Nyquist frequency, ω_N , such waves may not be observed, so further restrictions need be considered, namely, $\omega_0 \leq \omega_N$ has to hold. From (5.5) it follows that this condition is equivalent to

$$\sin^2 \theta \geq \frac{c^2}{v^2} \frac{\omega_N^2}{\omega_N^2 - \omega_{ac}^2} \Big|_{z=z_s}.$$

From this the minimum "observable" phase-speed can be evaluated:

$$\min v_{ph}^{obs} = \frac{vc}{\sqrt{\left(1 - \frac{\omega_{ac}^2}{\omega_N^2}\right) v^2 - c^2}} \Big|_{z=z_s} \quad (5.8)$$

⁵ sunquake egression signal is usually strong around $\nu = 6$ mHz

Therefore, in the acoustic wave-field excited by a vertical supersonic shock perturbation only waves with phase speed exceeding these will be observable. Moreover, as surface ripples from such source are determined by the phase speed, the minimum distance away from the source can be estimated using the above inequality. For example, if $c = 8\text{km/s}$, $v = 10\text{km/s}$, then minimum $v_{ph} \approx 13.3\text{km/s}$. For the Sun this corresponds to a skip-distance of around $5 - 7\text{ Mm}$. Let us take the value of cut-off frequency at source depth, $\omega_{ac}(z_s)/2\pi$, to be $\approx 5\text{ mHz}$. Then adding the condition that the cyclic frequency along the ray is no greater than 8.4 mHz , gives us a minimum phase speed estimate at $\approx 106\text{km/s}$. Therefore, in this case, only ripples at distances of order of hundred megameters from the source would be potentially observable.

More generally, let us rewrite (5.3):

$$\cos \gamma = \cos(\theta - \lambda) - \cos \theta \cos \lambda (1 - \cos \phi).$$

Then, as $\cos \theta$ and $\cos \lambda$ are non-negative, the inequality $\cos \gamma > c/v$ implies that $\cos(\theta - \lambda) > c/v > 0$. Hence,

$$\theta \in \left(\lambda - \arccos \frac{c}{v}, \lambda + \arccos \frac{c}{v} \right).$$

It is also clear $\cos \phi > c/v - \sin \theta \sin \lambda$. Thus for downward propagating source, i.e. $\lambda \in [0, \frac{\pi}{2}]$, very roughly it can be estimated $\cos \phi > c/v - \sin \lambda$, so only waves in the limited range of ϕ can be generated. But as rays propagate in the plane defined by z -axis and their initial wave-vector, this means that surface ripples will only appear in limited arcs in the direction of the source movement in this way producing anisotropy in wavefront amplitude.

Given supersonic movements observed at the sunquake source locations, and strong anisotropy in amplitude in the direction of the movement, it is tempting to hypothesise that this mechanism plays an important role in the sun-quake wavefront generation. However, caution needs to be exercised as the problem has been approached here from purely mathematical standpoint and the notoriously difficult question of method applicability has not been addressed. While this solution appears to provide a possible explanation for some of the observed properties of the sun-quake generated acoustic fields, the applicability of the method under the circumstances should be questioned as the variations are obviously very fast and known "sufficient" conditions for method applicability do not hold in this case (see Section 5.1.1). Numerical simulation or modal approach can provide a way to check this. It is interesting to note that published simulations showing generation of acoustic waves by convective vortices (Kitiashvili et al. 2011; Moll et al. 2011) also report supersonic movements at such vortices. Clearly further analysis is required to address these issues as well as to investigate various dependencies that in this paper were touched upon only briefly.

The anisotropy of flare generated acoustic wave-fronts has so far been attributed to the effects of magnetic field and more general plasma subsurface properties in the Active Regions where quakes take place. It is indisputable that such conditions affect and likely shape generated waves. However, it can be argued that the effects discussed in this paper, if supported by more realistic analysis as well as for magnetised case, can play an important role in determining the shape and properties of the wave-field, which is then inadvertently affected by the magnetic field, flows and other inhomogeneities along its path.

On the other hand, it can be seen that even without the magnetic field, e.g. when moving source is considered, the number of variables on which solution depends grows quite fast. Given our understanding of interaction of acoustic and magneto-acoustic waves, (see Schunker & Cally 2006; Moradi et al. 2010, and references

therein), it is clear that the inclusion of magnetic field effects is highly likely to paint an even more complex picture.

6 CONCLUSIONS

While the linear wave-equation has been extensively studied using geometric optics (see Kravtsov & Orlov 1990; Kravtsov & Orlov 1993, and references therein, for example), the non-linearity induced by the presence of acoustic-cutoff frequency in the Sun has often been overlooked. Using a point source as an example, in this paper I have shown how suitable description of initial conditions can be used to derive geometric properties of acoustic fields governed by such non-linear wave-equation. For stationary monochromatic source a full solution of the eikonal equation including Jacobian computation and phase function reconstruction was derived, showing dependency of the field shape on source depth and frequency. The general treatment of a moving source has also been outlined, analytically deriving some properties that might be associated with sun-quakes. While primarily concentrating on mathematical treatment to the problem, some intriguing properties of phase functions corresponding to near surface sources have been deduced. It was shown that due to the presence of acoustic cutoff frequency a shock travelling with supersonic speed can generate a cone-like wave-packet in the direction of the shock movement.

Given the asymptotic nature of the method used, the paper poses interesting and current questions about acoustic waves generated near the solar surface. The resolution of such questions will also shed further light on limits of applicability of the geometric asymptotics in solar applications.

The availability of the full solution including the Jacobian suggests a possibility of using it to compute the Green's function via solving of zero-order transport equation. This, however, is complicated by the presence of the caustics, which require separate treatment and classification as outlined in Kravtsov & Orlov (1990); Kravtsov & Orlov (1993). While this is a subject of future study, other methods such as outlined in Pérez Hernández & Gonzalez-Hernandez (2010); Lindsey et al. (2011, and references therein) might be better employed for this purpose.

Nonetheless, the method presented in this paper is shown to be a powerful tool for studying the behaviour of the wavefields when full initial conditions can be specified.

ACKNOWLEDGMENTS

I thank the referee, Dr Charles Lindsey, for his critical reading of the original version of the paper and many useful comments and suggestions that improved the presentation of the paper. I also acknowledge the Leverhulme Trust for funding the Probing the Sun: inside and out project upon which this research is based.

REFERENCES

- Arnold V. I., 1978, *Mathematical methods of classical mechanics*, Arnold, V. I., ed.
- Barnes G., Cally P. S., 2001, *PASA*, 18, 243
- Bogdan T. J., 1997, *Astrophysical Journal*, 477, 475
- Bogdan T. J., Cally P. S., 1995, *ApJ*, 453, 919
- Chapman S. J., Lawry J. M. H., Ockendon J. R., Tew R. H., 1999, *SIAM Review*, 41, 417

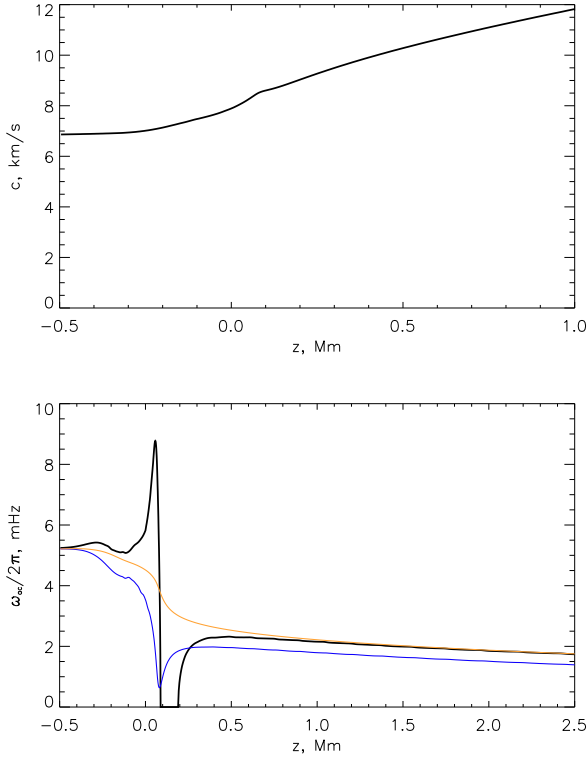


Figure 6. Adiabatic soundspeed (left) and acoustic cut-off frequency (right, black line) from Christensen-Dalsgaard model C in the upper layers of solar interior. Note that the negative part of ω_{ac}^2 has been truncated at zero. Yellow line is the isothermal cut-off frequency deduced from the model, $\frac{c^2}{4H_p^2}$, blue line represents $\frac{c^2}{4H_p^2}$.

- Christensen-Dalsgaard J., 2003, 268
 Christensen-Dalsgaard J. et al., 1996, *Science*, 272, 1286
 Couvidat S., Birch A. C., Kosovichev A. G., 2006, *ApJ*, 640, 516
 Couvidat S., Birch A. C., Kosovichev A. G., Zhao J., 2004, *ApJ*, 607, 554
 Donea A., 2011, *Space Sci. Rev.*, 158, 451
 Donea A., Braun D. C., Lindsey C., 1999, *ApJ*, 513, L143
 Donea A., Lindsey C., 2005, *ApJ*, 630, 1168
 D'Silva S., 1996, *Astrophysical Journal* v.462, 462, 519
 D'Silva S., Duvall T. L., 1995, *Astrophys J*, 438, 454
 Duvall, Jr. T. L., Jefferies S. M., Harvey J. W., Pomerantz M. A., 1993, *Nature*, 362, 430
 Felsen L. B., Marcuvitz N., 1991, *Radiation and Scattering of Waves*. New York, USA: Wiley-IEEE
 Giles P. M., 2000, PhD thesis, STANFORD UNIVERSITY
 Gough D. O., 1993, in *Astrophysical Fluid Dynamics - Les Houches 1987*, J.-P. Zahn & J. Zinn-Justin, ed., pp. 399–560
 Gough D. O., 2007, *Astronomische Nachrichten*, 328, 273
 Guillemin V., Sternberg S., 1990, 480
 Kitiashvili I. N., Kosovichev A. G., Mansour N. N., Wray A. A., 2011, *ApJ*, 727, L50
 Kosovichev A. G., 2006, *Sol. Phys.*, 238, 1
 Kosovichev A. G., 2007, *ApJ*, 670, L65
 Kosovichev A. G., 2011, *ApJ*, 734, L15+
 Kosovichev A. G., Duvall, Jr. T. L., 1997, in *Astrophysics and Space Science Library*, Vol. 225, SCOR'96 : Solar Con-

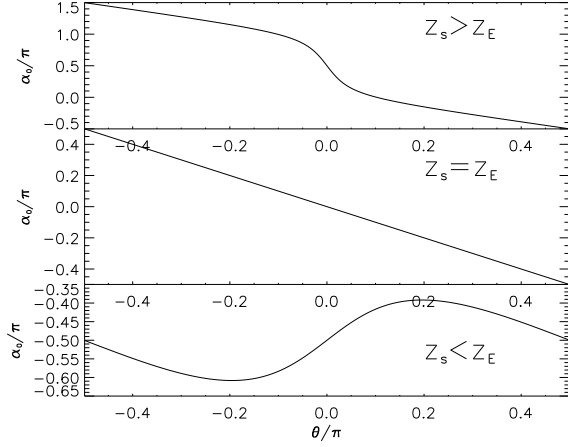


Figure 7. Example of the relationship between θ and α_0 for stationary monochromatic source for $\xi = 1.8$ (top), $\xi = 2$ (middle), $\xi = 4$ (bottom).

- vection and Oscillations and their Relationship, F. P. Pijpers, J. Christensen-Dalsgaard, & C. S. Rosenthal, ed., pp. 241–260
 Kosovichev A. G., Zharkova V. V., 1998, *Nature*, 393, 317
 Kravtsov Y. A., Orlov Y. I., 1990, *Geometrical Optics of Inhomogeneous Media*. Berlin, GR: Springer-Verlag
 Kravtsov Y. A., Orlov Y. I., 1993, *Caustics, Catastrophes and Wave Fields*. Berlin, GR: Springer-Verlag
 Lindsey C., Braun D., Hernández I., Donea A., 2011, in 'Holography. Different fields of Application', F. A. M. Ramirez, ed., p. 81
 Lindsey C., Braun D. C., 2000, *Sol. Phys.*, 192, 261
 Lindsey C., Braun D. C., 2000, *Science*, 287, 1799
 Lindsey C., Braun D. C., 2004, *The Astrophysical Journal Supplement Series*, 155, 209
 Lindsey C., Donea A., 2008, *Sol. Phys.*, 251, 627
 Matthews S. A., Zharkov S., Zharkova V. V., 2011, *ApJ*, 739, 71
 Moll R., Cameron R. H., Schüssler M., 2011, *A&A*, 533, A126
 Moradi H. et al., 2010, *Sol. Phys.*, 267, 1
 Moradi H., Donea A., Lindsey C., Besliu-Ionescu D., Cally P. S., 2007, *MNRAS*, 374, 1155
 Pérez Hernández F., Gonzalez-Hernandez I., 2010, *The Astrophysical Journal*, 711, 853
 Schunker H., Cally P. S., 2006, *Mon Not R Astron Soc*, 372, 551
 Shelyag S., Zharkov S., Fedun V., Erdélyi R., Thompson M. J., 2009, *A&A*, 501, 735
 Thompson M. J., Zharkov S., 2008, *Sol. Phys.*, 251, 225
 Zharkov S., Green L. M., Matthews S. A., Zharkova V. V., 2011a, *ApJ*, 741, L35
 Zharkov S., Green L. M., Matthews S. A., Zharkova V. V., 2012, *Sol. Phys.*, 292
 Zharkov S., Zharkova V. V., Matthews S. A., 2011b, *ApJ*, 739, 70
 Zharkova V. V., Zharkov S. I., 2007, *ApJ*, 664, 573

APPENDIX A: MONOCHROMATIC POINT SOURCE: EIKONAL SOLUTION FOR POLYTROPE MODEL

A1 Characteristics

In this section the eikonal equation for polytrope model is solved using the monochromatic point source initial conditions deduced in Section 3.2. For given frequency, ω , and source depth, z_s , we

reconstruct the graph of the phase function, φ , throughout the phase space domain in terms of ray-coordinates using group travel-time as the parameter along the ray. The Jacobian of the transform from ray to Cartesian coordinates is evaluated, and the phase function is reconstructed.

Without loss of generality, take $x_s = 0$ and $\omega > 0$. By construction (see Section 3.2), $k_h \geq 0$ and $\theta \in (-\frac{\pi}{2}, \frac{\pi}{2})$. Note that by our definition (see Figure 1) θ is zero in the horizontal direction and is increasing clock-wise. For fixed z_s, ω , the initial values for wavevector components are determined in terms of the take-off angle, θ , and given by $k_{h0} = k_s(z_s, \omega) \cos \theta$, $k_{z0} = k_s(z_s, \omega) \sin \theta$. Using the corresponding upper and lower turning points, in accordance with (4.3), define

$$a(\theta|\omega, z_s) = \frac{1}{2} \frac{\omega^2 m}{k_s^2 g} (1 + \tan^2 \theta)$$

and

$$b^2(\theta|\omega, z_s) = a^2 - \frac{m(m+2)}{4k_h^2}.$$

Then, in view of (4.5b), the solution can be written as

$$\begin{cases} x = \frac{1}{2} \frac{\omega}{k_h} t_g - b(\cos \alpha - \cos \alpha_0), & \text{(A1a)} \\ z = a + b \sin \alpha, & \text{(A1b)} \\ t = t_g + t_0, & \text{(A1c)} \\ \alpha(t_g, \theta|\omega, z_s) = \frac{k_h g}{\omega m} t_g + \alpha_0, & \text{(A1d)} \\ \alpha_0(\theta|\omega, z_s) = \sin^{-1} \left(\frac{z_s - a}{b} \right). & \text{(A1e)} \end{cases}$$

From this it is immediately clear that for an individual ray upper turning points correspond to the values $\alpha = -\frac{\pi}{2} + 2n\pi$, while lower turning points are given by $\alpha = \frac{\pi}{2} + 2n\pi$, where $n = 0, 1, 2, \dots$. The horizontal distance between two successive bounces on the surface, called a skip-distance, is $\Delta(k_h, \omega) = 2\pi a = \pi \omega^2 m / k_h^2 g = v_{ph}^2 \pi m / g$, where $v_{ph} = \omega / k_h$ is the horizontal phase-speed. The time, t_Δ , it takes the ray to travel between the bounces is linked to the distance: $\Delta = g t_\Delta^2 / 4\pi m$.

Since $\omega > 0$, α is increasing when t_g is increasing. With ω constant on the phase function graph, and $k_h = k_{h0} = k_s \cos \theta$ constant along the ray, we need to find k_z in ray-coordinates to complete the solution (A1a-A1c) to phase space. This is found from the condition that Hamiltonian (2.8a) is zero. Indeed from (4.3) and (A1b) it follows that $k_z = k_h b \cos \alpha / z$, with the choice of the square root branch taken care of by Some care should be taken in choosing the correct branch of the square root, which is addressed via a choice of the inverse sine branch in the definition of α_0 (A1e) as follows. For given z_s, ω and θ , there will be two solutions for parameter $\alpha_0(\theta)$: $\alpha_0^+ \in [-\frac{\pi}{2}, \frac{\pi}{2}]$ and $\alpha_0^- = \pi - \alpha_0^+ \in [\frac{\pi}{2}, \frac{3\pi}{2}]$. The former clearly corresponds to rays going down from the source, z increasing with t_g , $k_{z0} > 0$, and the latter to rays going up (z decreasing, $k_{z0} < 0$). Thus, α_0^+ is chosen when $\theta > 0$, and α_0^- when $\theta < 0$. To ensure smooth dependence of α_0 on θ , one has to join the two solutions at $\theta = 0$, which corresponds to $k_{z0} = 0$, i.e. the ray that has source depth, z_s , as one of its turning points. In view of the Proposition 1 and Corollary 1 in Section 4.1, where a partition depth is deduced and determined for polytrope model, depending on whether the source is located above or below the partition depths z_E , this turning point will be either upper ($\alpha_0 = \frac{\pi}{2} + 2n\pi$) or lower ($\alpha_0 = -\frac{\pi}{2} + 2n\pi$).

To treat this mathematically, let us define

$$\xi = \frac{\omega^2}{\omega^2 - \omega_{ac}^2} \Big|_{z=z_s}.$$

The condition that waves are not evanescent, $k_s^2 > 0 \iff \omega > \omega_{ac}(z_s)$, implies that $\xi \in (1, \infty)$. When $z_s = z_E$, $\xi = 2$. It is helpful to rewrite

$$\begin{aligned} a &= \frac{\xi}{2 \cos^2 \theta} z_s, \\ b^2 &= \frac{z_s^2}{4 \cos^4 \theta} ((\xi - 2)^2 + 4(\xi - 1) \sin^2 \theta). \end{aligned}$$

Note that $b = 0$ only when both $\xi = 2$ and $\theta = 0$. When $b \neq 0$, $b \sin \alpha_0 = z_s - a$ and $b \cos \alpha_0 = z_s k_{z0} / k_h = z_s \tan \theta$, so that

$$\tan \alpha_0 = \frac{1 - \frac{\xi}{2}}{\tan \theta} - \frac{\xi}{2} \tan \theta = \cot \theta - \frac{\xi}{\sin 2\theta}.$$

Consider the behaviour at $\theta = 0$, as well as θ approaching edge points, $-\frac{\pi}{2}, \frac{\pi}{2}$, that can be potentially problematic. There are three cases:

- $z_s > z_E, \xi \in (1, 2) \implies \theta = 0$ corresponds to lower turning point. Thus chose $\alpha_0(\theta = 0) = \frac{\pi}{2}$. Then, $\alpha_0 \rightarrow -\frac{\pi}{2}^-$ as $\theta \rightarrow \frac{\pi}{2}^-$; and $\alpha_0 \rightarrow \frac{3\pi}{2}^+$ as $\theta \rightarrow -\frac{\pi}{2}^+$;
- $z_s < z_E, \xi \in (2, \infty) \implies \theta = 0$ corresponds to upper turning point. Thus chose $\alpha_0(\theta = 0) = -\frac{\pi}{2}$. Then, $\alpha_0 \rightarrow -\frac{\pi}{2}^-$ as $\theta \rightarrow \frac{\pi}{2}^+$; and $\alpha_0 \rightarrow -\frac{\pi}{2}^+$ as $\theta \rightarrow -\frac{\pi}{2}^+$;
- $z_s = z_E, \xi = 2, \tan \alpha_0 = -\tan \theta$, when $\theta \neq 0$. For $\theta = 0$ the value of α_0 is not defined, but as $a = z_E$, let us choose $\alpha_0(\theta = 0) = 0$ with $\alpha_0 \rightarrow -\frac{\pi}{2}^+$ as $\theta \rightarrow \frac{\pi}{2}^-$; and $\alpha_0 \rightarrow \frac{\pi}{2}^+$ as $\theta \rightarrow -\frac{\pi}{2}^+$;

Therefore, using formulas for $b, \tan \alpha_0$ and $\cos \alpha_0$, the derivative of α_0 by θ can be expressed in terms of ξ :

$$\begin{aligned} \frac{\partial \alpha_0}{\partial \theta} &= \frac{2(\xi - 2) - 4(\xi - 1) \sin^2 \theta}{(\xi - 2)^2 + 4(\xi - 1) \sin^2 \theta} \\ &= -1 + \frac{\xi(\xi - 2)}{(\xi - 2)^2 + 4(\xi - 1) \sin^2 \theta}. \end{aligned} \quad \text{(A3)}$$

In the case when $z_s = z_E, \xi = 2$, the above formula takes form $\frac{\partial \alpha_0}{\partial \theta} = -1$. For fixed frequency and source depth, taking into account the information above, relationship (A3) can be integrated to find

$$\alpha_0(\theta) = \begin{cases} \frac{\pi}{2} - \theta + \tan^{-1} \left(\frac{\xi}{\xi - 2} \tan \theta \right) & z_s > z_E, \xi \in (1, 2), \\ -\frac{\pi}{2} - \theta + \tan^{-1} \left(\frac{\xi}{\xi - 2} \tan \theta \right) & z_s < z_E, \xi \in (2, \infty) \\ -\theta & z_s = z_E, \xi = 2. \end{cases} \quad \text{(A4)}$$

Representative plots for α_0 as function of θ are shown in Figure 7.

A2 Caustics

Equations (A1a-A1d) together with with

$$k_h = k_s(\omega, z_s) \cos \theta, \quad \text{(A5a)}$$

$$k_z = k_h \frac{b \cos \alpha}{z}, \quad \text{(A5b)}$$

$$\omega = \text{const}, \quad \text{(A5c)}$$

define the three-dimensional graph of φ lying in ΩM in terms of ray coordinates (θ, t_0, t_g) . As $t = t_g + t_0$ and since neither x nor

z depend explicitly on t_0 , the Jacobian of the coordinate transform can be written as

$$\mathcal{D} = \frac{\partial(x, z, t)}{\partial(\theta, t_0, t_g)} = \begin{vmatrix} \frac{\partial x}{\partial \theta} & 0 & \frac{c^2}{\omega} k_h \\ \frac{\partial z}{\partial \theta} & 0 & \frac{c^2}{\omega} k_z \\ 0 & 1 & 1 \end{vmatrix} = -\frac{\partial(x, z)}{\partial(\theta, t_g)} \quad (\text{A6})$$

Note that $\mathcal{D} = 0$ when the wave-vector $(\partial x/\partial t_g, \partial z/\partial t_g)$ is tangent to the wavefront, i.e. collinear to $(\partial x/\partial \theta, \partial z/\partial \theta)$.

When $\theta \in (-\frac{\pi}{2}, \frac{\pi}{2}) \Rightarrow k_h \neq 0$, α can be used instead of t_g as a parameter along the ray:

$$\mathcal{D} = \frac{\partial(x, z, t)}{\partial(\theta, t_0, \alpha)} \times \frac{\partial(\theta, t_0, \alpha)}{\partial(\theta, t_0, t_g)} = -\frac{k_h g}{\omega m} \frac{\partial(x, z)}{\partial(\theta, \alpha)}. \quad (\text{A7})$$

Let us consider the general case $z \neq z_E$. Making use of the formulas

$$\begin{aligned} \frac{\partial k_h}{\partial \theta} &= -k_h \tan \theta, \quad \frac{\partial a}{\partial \theta} = 2a \tan \theta, \\ \frac{\partial b}{\partial \theta} &= \frac{\tan \theta}{b} (a^2 + b^2) \text{ when } z_s \neq z_E, \\ \frac{\partial \alpha}{\partial \theta} &= -(\alpha - \alpha_0) \tan \theta + \frac{\partial \alpha_0}{\partial \theta}, \end{aligned}$$

the partial derivatives with respect to take-off angle are evaluated:

$$\begin{cases} \frac{\partial x}{\partial \theta} = (\alpha - \alpha_0) \tan \theta (a - b \sin \alpha) \\ \quad + z_s (1 + \tan^2 \theta) - \frac{\tan \theta}{b} (a^2 + b^2) \cos \alpha \\ \quad + b \sin \alpha \frac{\partial \alpha_0}{\partial \theta} \end{cases} \quad (\text{A9a})$$

$$\begin{cases} \frac{\partial z}{\partial \theta} = 2a \tan \theta + \frac{\tan \theta}{b} (a^2 + b^2) \sin \alpha \\ \quad - (\alpha - \alpha_0) b \cos \alpha \tan \theta + b \cos \alpha \frac{\partial \alpha_0}{\partial \theta} \end{cases} \quad (\text{A9b})$$

$$\frac{\partial x}{\partial t_g} = \frac{k_h g}{\omega m} (a + b \sin \alpha), \quad (\text{A9c})$$

$$\frac{\partial z}{\partial t_g} = \frac{k_h g}{\omega m} b \cos \alpha \quad (\text{A9d})$$

Then using α as a parameter along the ray define the scaled jacobian

$$\begin{aligned} J(\theta, \alpha) &= \frac{\omega m}{k_h g} \mathcal{D} = b \cos \alpha \times \\ &\times \left(2a(\alpha - \alpha_0) \tan \theta - a \frac{\partial \alpha_0}{\partial \theta} + z_s (1 + \tan^2 \theta) \right) \\ &- \frac{\tan \theta}{b} ((a^3 + 3b^2 a) \sin \alpha + 3a^2 b + b^3). \end{aligned} \quad (\text{A10})$$

A3 Reconstructing phase function φ

Using α as a parameter along the ray and taking into account (2.8a), phase function derivative along the ray (2.10) takes the form

$$\frac{d\varphi}{d\alpha} = k_h \frac{dx}{d\alpha} + k_z \frac{dz}{d\alpha} - \omega \frac{dt}{d\alpha} = -\frac{z}{k_h} \frac{\omega_{ac}^2}{c^2}.$$

This is then integrated to reconstruct the phase function along the ray

$$\begin{aligned} \varphi &= \varphi_0 - \frac{m(m+2)}{4k_h} \int_{\alpha_0}^{\alpha} \frac{d\alpha'}{a + b \sin \alpha'} \\ &= \varphi_0 - \frac{1}{\sqrt{m(m+2)}} \left[\tan^{-1} \left(\frac{a}{\sqrt{z_u z_l}} \tan \frac{\alpha}{2} + \frac{b}{\sqrt{z_u z_l}} \right) \right. \\ &\quad \left. - \tan^{-1} \left(\frac{a}{\sqrt{z_u z_l}} \tan \frac{\alpha_0}{2} + \frac{b}{\sqrt{z_u z_l}} \right) \right] \end{aligned} \quad (\text{A11})$$

This paper has been typeset from a $\text{\TeX}/\text{\LaTeX}$ file prepared by the author.